AIDA-2020-CONF-2016-008

AIDA-2020

Advanced European Infrastructures for Detectors at Accelerators

Conference/Workshop Paper

Technology developments and first measurements on inverse Low Gain Avalanche Detector (iLGAD) for high energy physics applications

Carulla, M. (IMB-CNM (CSIC)) *et al*

07 December 2016

The AIDA-2020 Advanced European Infrastructures for Detectors at Accelerators project has received funding from the European Union's Horizon 2020 Research and Innovation programme under Grant Agreement no. 654168.

This work is part of AIDA-2020 Work Package **7: Advanced hybrid pixel detectors**.

The electronic version of this AIDA-2020 Publication is available via the AIDA-2020 web site <http://aida2020.web.cern.ch> or on the CERN Document Server at the following URL: <http://cds.cern.ch/search?p=AIDA-2020-CONF-2016-008>

Copyright © CERN for the benefit of the AIDA-2020 Consortium

Technology developments and first measurements on inverse Low Gain Avalanche Detector (iLGAD) for high energy physics applications

M. Carulla[a,*], M. Fernández-García[b], P. Fernández-Martínez[a], D. Flores[a], J. González[b], S. Hidalgo[a], R. Jaramillo[b], A. Merlos[a], F.R. Palomo[c], G. Pellegrini[a], D. Quirion[a] and I. Vila[b]

[a] *Centro Nacional de Microelectrónica, IMB-CNM (CSIC) ,*
C/ dels Til·lers, Campus UAB, Cerdanyola del Vallès, 08193 Barcelona, Spain

[b] *Instituto de Física de Cantabria IFCA-CSIC-UC,*
Edificio Juan Jordá, Avenida de los Castros, 39005 Santander, Spain

[c] *Escuela Técnica Superior de Ingeniería. Universidad de Sevilla*
Camino de los Descubrimientos. Isla de la Cartuja, 41092 Sevilla, Spain

[*] *E-mail*: mar.carulla@imb-cnm.csic.es

ABSTRACT: The first Inverse Low Gain Avalanche Detector (iLGAD) have been fabricated at IMB-CNM (CSIC). The iLGAD structure includes the multiplication diffusions at the ohmic contact side while the segmentation is implemented at the front side with multiple P^+ diffusions. Therefore, iLGAD is P on P position-sensitive detector with a uniform electric field all along the device area that guarantees the same signal amplification wherever a particle passes through the sensitive bulk solving the main draw of the LGAD microstrip detector. However, the detection current is dominated by holes flowing back from the multiplication junction with the subsequent transient current pulse duration increase in comparison with conventional LGAD counterparts. Applications of iLGAD range from tracking and timing applications like determination of primary interaction vertex to medical imaging. The paper addresses the optimization of the iLGAD structure with the aid of TCAD simulations, focusing on the electric field profiles of iLGAD and LGAD microstrip structures and the corresponding gain. The electrical performance of the first fabricated samples is also provided. For the first time, we have experimental demonstrate the signal amplification of this novel iLGAD detectors.

KEYWORDS: Solid state detectors; Particle tracking detectors; Timing detectors; Avalanche multiplication , Radiation-hard detectors.

1

Contents

1. Introduction 1
2. iLGAD Structure and Process Techonolgy ¡Error! Marcador no definido.
3. TCAD Optimization 3
4. Electrical Characterization 4
5. Experimental Observation of Charge Multiplication 5
6. Conclusion 7

9
10

1. Introduction

12 Conventional avalanche detectors [1] integrated on P-type high resistivity substrates are based
13 on the local high electric field region where charge multiplication can take place. Electrons
14 generated by an incident particle in the depleted Silicon volume flows to the positively biased
15 shallow N-type diffusion and secondary ionization is found at the N^+/P^- junction, provided the
16 electric field peak is high enough. These detectors derive from the PiN diode structure where no
17 multiplication is found until the reverse bias approaches the breakdown voltage of the device
18 with the subsequent sharp increase of the gain. PiN detectors provide information about energy
19 and position of the incident particles but the signal-to-noise ratio (SNR) is poor. Indeed, the
20 maximum reverse voltage capability of conventional detectors varies with the accumulated
21 radiation damage leading to possible device failure.

22 LGAD (Low Gain Avalanche Detector) structure [2] is designed to exhibit a moderate
23 gain with an almost linear evolution in a wide range of reverse voltage values. Moreover,
24 microstrip and pixel detector layouts with fine segmentation pitches can be easily obtained with
25 the LGAD approach with high SNR when compared with PiN detector. Therefore, precise
26 measurements of energy, position and time of arrival of the incident particles can be achieved
27 with LGAD designs. The process technology and design issues of LGAD detectors fabricated
28 on 300 μm substrates have already been discussed in the past [3]. Pad, pixel and microstrip
29 detectors have already been fabricated with voltage capability in excess of 1000 V, extremely
30 low leakage current values and gain in the 5 to 20 range. However, thick LGAD detectors suffer
31 from severe gain reduction when submitted to fluences higher than 1×10^{14} cm^{-2} due to
32 displacement damage [4], which limits their use in extremely high radiation environments.
33 However, microstrip and pixel LGAD detectors are good for tracking and timing, primary
34 interaction vertex and medical applications where a high SNR is mandatory. Indeed, the LGAD
35 architecture can be applied to thin substrates (Silicon-on-Insulator with active Silicon layers of
36 some tenths of microns) [5], although a further optimization of the layout and the process
37 technology is needed.

38 Fabricated microstrip LGAD detectors exhibit non-uniform gain through each single
39 strip since the necessary P-type diffusion to provide multiplication is locally implanted in the

central part of the strip. The iLGAD (Inverse LGAD) structure was developed for microstrip and pixel designs with uniform gain. Initial optimization of the iLGAD structure was already performed [6]. This paper describes the technology, the experimental performance and the charge collection measurements of the first fabricated iLGAD detectors.

2. iLGAD Structure and Process Technology

Microstrip LGAD detectors were initially designed to be fully compatible with the standard LGAD technology. The core LGAD microstrip schematic cross-section is plotted in Figure 1 (left) were three strips are included with a P-stop diffusion in between to prevent the formation of a surface inversion layer. N on P microstrips are implemented with a shallow N^+ diffusion overlapping the P-type multiplication diffusion. LGAD microstrips were fabricated with a total detection area of 1 cm² and two different strip layouts: pitch of 80 µm, N^+ diffusion of 32 and multiplication diffusion of 20 µm and pitch of 160 µm, N^+ diffusion of 112 µm and multiplication diffusion of 100 µm. Although the detectors had a voltage capability in the range of 1000 V and a gain in the range of 10 in the center of the strip, strong gain decay was observed at the edge of the strip [6]. This is basically due to the local multiplication diffusion, which is narrower than the shallow N^+ contact diffusion.

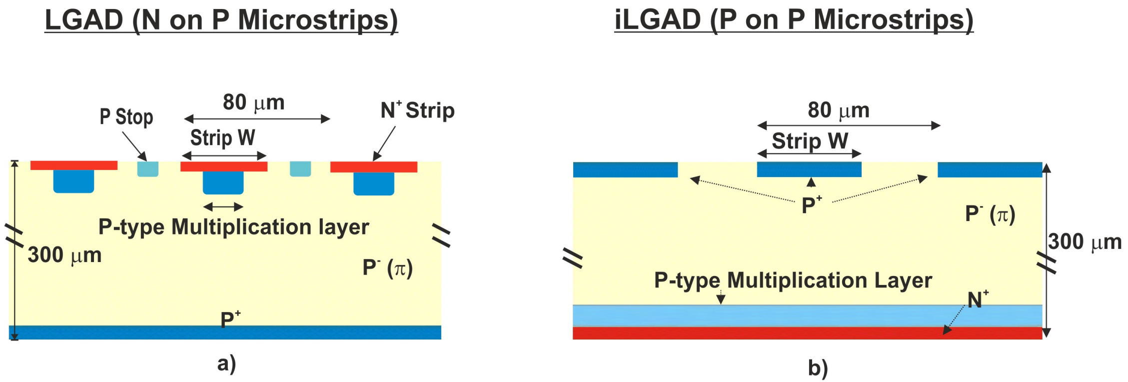

Figure 1: Cross-sections of the core layout of LGAD (left) and iLGAD (right) microstrip designs.

The iLGAD structure is also based on the conventional LGAD process technology but the segmentation is now located at the P^+ side, according to the schematic cross-section of the core iLGAD depicted in Figure 1 (right). Therefore, the multiplication diffusions are no longer locally performed and the gain is the same through the strip providing a position-sensitive detector with uniform amplification wherever a particle hits the detector. Holes generated in the depleted Silicon volume immediately flow towards the P^+ strips while electrons flow towards the multiplication region where additional holes are generated reaching the P^+ strips after traveling back through the depleted region. As a consequence, the collecting time is larger in the iLGAD P on P miscrostrips when compared with the equivalent N on P LGAD microstrips.

The cross-section of the iLGAD structure is shown in Figure 2, where the different diffusions and the periphery of the device are clearly detailed. The multiplication junction is protected by a JTE N-type diffusion surrounding the multiplication area to ensure a high voltage capability. The back side metal is only placed at the edge of the mutiplication area for not masking the incident particles while the top side metal is segmented to define the microstrips. Finally, a P^+ diffusion surrounding the microstrip area is implemented to extract the leakage current generated at the device periphery. Although the iLGAD process technology requires

75 double side alignment and four additional mask layers, diffusion, implantation and thermal steps
76 are identical to those used in the LGAD fabrication process.
77

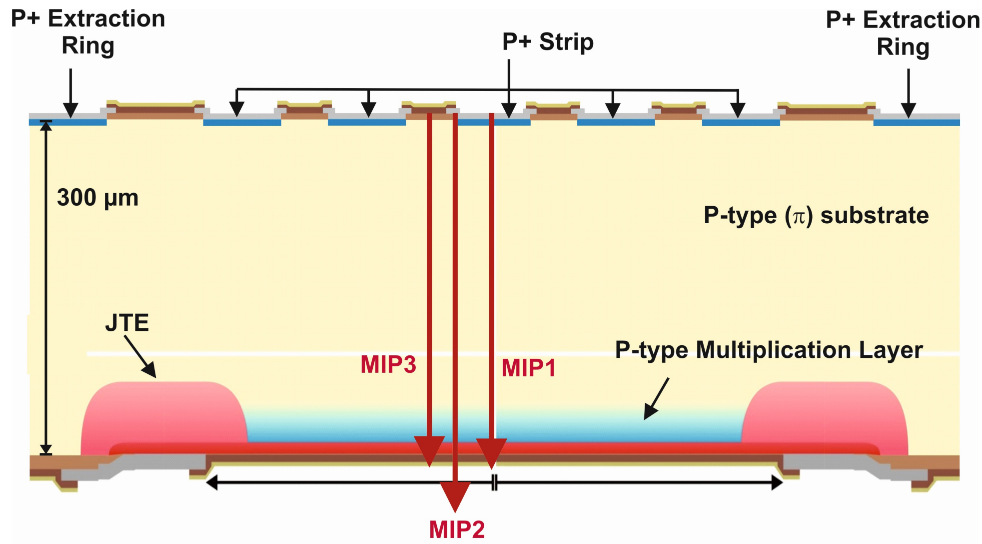

78
79 **Figure 2:** Cross-sections of the complete iLGAD structure including edge termination and extraction
80 rings. Simulated paths of incident MIP particles are also indicated.

81 ## 3. TCAD Optimization

82 The iLGAD optimization was performed once the doping profiles of the multiplication junction
83 are in agreement with those obtained from the LGAD fabrication process with the aid of
84 Secondary Ion Mass Spectrometry (SIMS) technique. Microstrip LGAD and iLGAD structures
85 were simulated in a 300 µm lowly doped P-type substrate to compare the gain uniformity in the
86 strips and its relation with the electric field distribution.

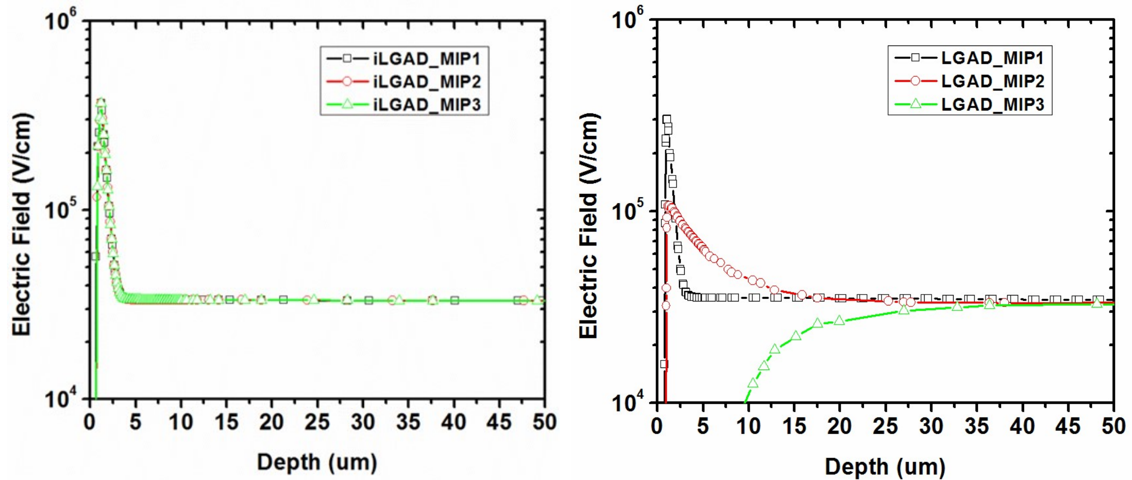

87
88
89 **Figure 3:** Simulated electric field distribution at the first 50 µm of the multiplication side in the three
90 incident particle paths depicted in Figure 2 for iLGAD (left) and LGAD (right) at 1000 V.
91

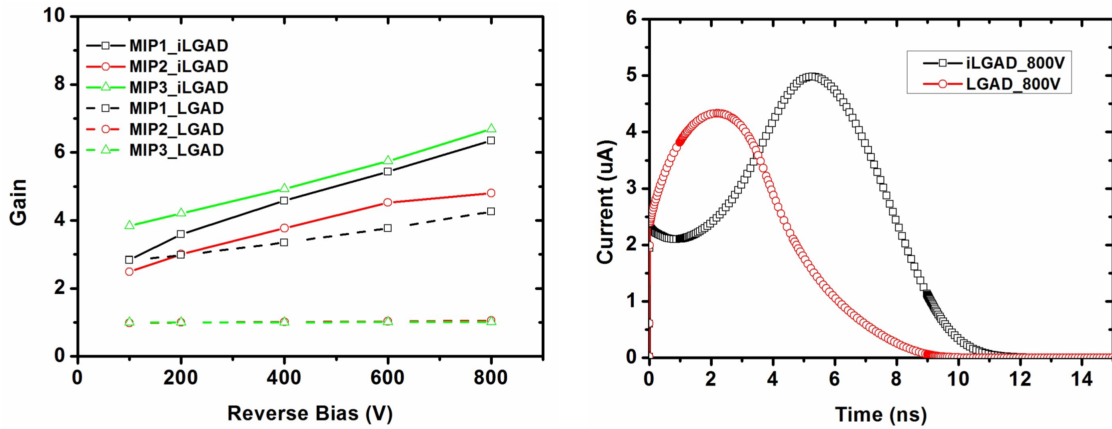

Figure 4: Simulated gain evolution versus the applied reverse voltage for iLGAD and LGAD microstrips as a function of the incident particle path (left) and simulated transient charge collection at the center of the strip for iLGAD and LGAD structures at 800 V (right).

The simulated electric field distribution at the multiplication side for the three incident particle paths depicted in Figure 2 is provided in Figure 3 at a reverse voltage of 1000 V. The electric field distributions corresponding to the iLGAD microstips shows no difference between the center of the strip, the edge of the strip and the inter-strip locations, thus providing a uniform gain performance. On the contrary, the simulated electric field distributions corresponding to the LGAD microstrips have a very different shape depending on the incident particle path. At the center of the strip the electric field shape is the expected for multiplication but at the edge of the strip and at the inter-strip regions there are no electric field peak and no multiplication can be expected.

The comparison of the simulated gain evolution versus the applied reverse voltage in iLGAD and LGAD microstrip structures is provided in Figure 4 (left). In the iLGAD microstrips case, the simulated gain exhibits an almost linear evolution with slight difference between the incident particle paths, ranging from 3 to 8. However, the LGAD microstrip structure only exhibits gain if the particle hits the center of the strip. The simulated charge collection evolution when the incident particle hits the center of the strip for iLGAD and LGAD microstrips is shown in Figure 4 (right) at a reverse voltage of 800 V. The charge collection is much faster in the LGAD case since the current is basically due to the electrons reaching the N^+ diffusion, although a tail can be distinguished as a consequence of the holes flowing back from the multiplication N^+P junction to the P^+ contact. In the iLGAD case, the current mainly corresponds to the holes flowing back from the multiplication N^+P junction. The use of thinner substrates will help in reducing the collecting time of the iLGAD structure.

4. Electrical Characterization

Fabricated iLGAD structures with pitch values of 80 and 160 μm have been extensively characterised to obtain the electrical and detection performances. Different implantation doses were used for the creation of the P-type multiplication diffusion to determine the optimum process technology in terms of minimum leakage current and highest gain in the linear region. The experimental reverse blocking performance of iLGAD pad detectors from two wafers with different implantation doses, close to the optimum value, are shown in Figure 5 (left). The

125 measured leakage current of the iLGAD devices is in the range of 100-200 nA with a voltage
126 capability higher than 900 V.

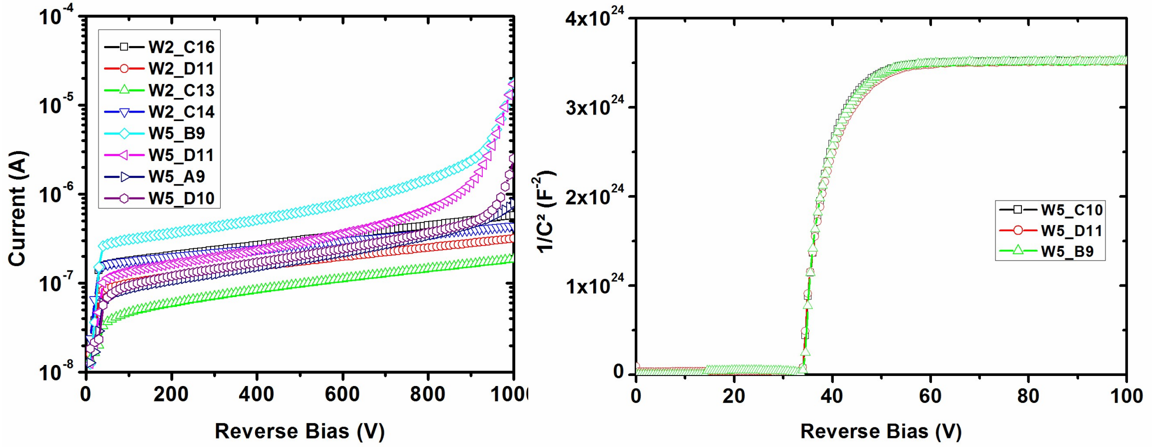

127

128 **Figure 5**. Experimental reverse blocking characteristics of three iLGAD microstrip detectors with a
129 detection area of 1.3x1.3 mm^2 for two different implantation doses of the multiplication diffusion (left)
130 and experimental capacitance evolution in three iLGAD microstrip detectors (right).

131 The capacitance measurements on three different iLGAD microstrip devices from the
132 wafer with the optimum implantation dose for the multiplication diffusion are shown in Figure 5
133 (right). The full depletion of the P-type multiplication diffusion is achieved at 35 V while the
134 full depletion of the high resistivity substrate is found at 70 V.

135 5. Experimental Observation of Charge Multiplication

136 A distinct and unambiguous signature of the presence of electron-driven avalanche
137 multiplication can be obtained from the shape of the transient-current induced by the injection
138 of electrons into the P^+ ohmic side. Such transient current presents two very distinct parts.
139 Initially, the early current is dominated by the drift of the primary carriers (electrons) towards
140 the multiplication junction; then, once the primary carriers reach that junction, the impact
141 ionization and the consequent avalanche carrier multiplication starts; at this time, the secondary
142 holes become dominant in the transient current; eventually, all the holes are collected at the P^+
143 ohmic side and the transient current goes back to the DC level.
144 Electron injection experiments have been carried out using a conventional TCT system [7]
145 where the non-equilibrium charge carriers are generated by means of a picosecond red laser and
146 being the microstrip signal read through a channel whose bandwidth is limited by the detector
147 capacitance [8]. Three different detectors have been tested: a microstrip N on P detector (W2-
148 G9) without multiplication, a microstrip LGAD N on P detector (W3-H6) and a microstrip
149 iLGAD P on P detector.
150 As it is well known, the observed transient current can be described by means of the
151 Ramo's theorem. In Figure 6 it is shown the transient current induced by a laser light with a
152 low-penetrating wavelength (670 nm) and with the laser beam impinging on the non-segmented
153 P^+ ohmic side of a standard microstrip PiN detector with a layout identical to that of a
154 microstrip LGAD. The observed current waveform is very peaked towards the end of the
155 electron drift as expected from the Ramo's theorem since both the weighting and the electric

field are very peaked near the strip-like electrode; the primary electrons mostly induce this transient current.

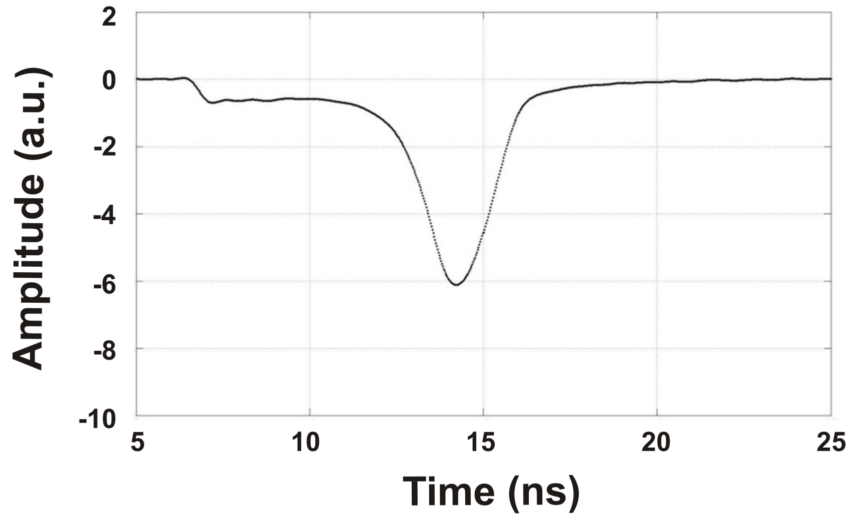

Figure 6. Transient-current waveform corresponding to the electron injection into a PiN N on P microstrip detector (W2-G9).

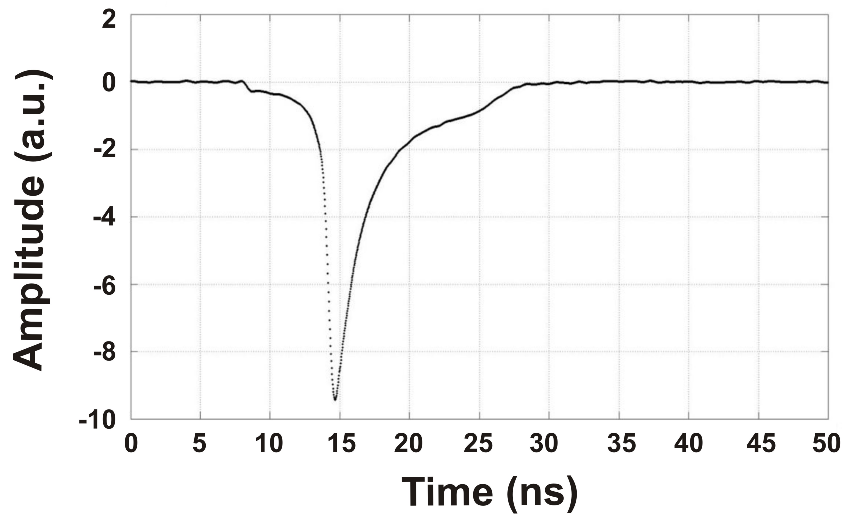

Figure 7. Transient-current waveform corresponding to the electron injection into an N on P microstrip LGAD detector (W3-H6).

The analogous electron-injection transient-current waveform for a microstrip LGAD detector can be observed in Figure 7. As already stated, the waveform duration is significantly longer since now both primary electrons and secondary holes are contributing to the signal. The drift of the electrons towards the segmented multiplication junction dominates the first part of the transient-current waveform, up to about 15 ns. Once the electrons reach that junction the avalanche process starts and secondary holes are then drifted towards the P^+ ohmic side and inducing the second part of the waveform. For this device, the closeness of the electric and weighting field peaks to the multiplication P-type diffusion makes the electron-injection waveform very peaked around the multiplication onset time.

175
176

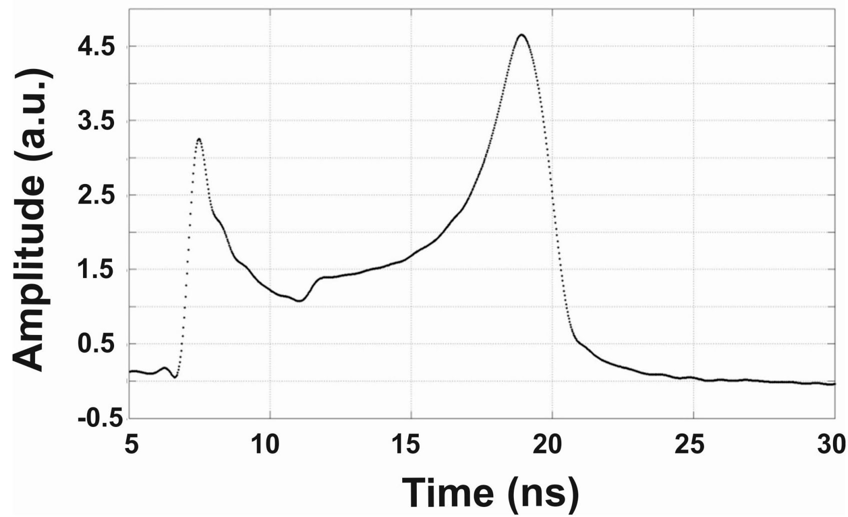

177 **Figure 8**. Transient-current waveform corresponding to the electron injection into a P on P microstrip
178 iLGAD detector.

179
180

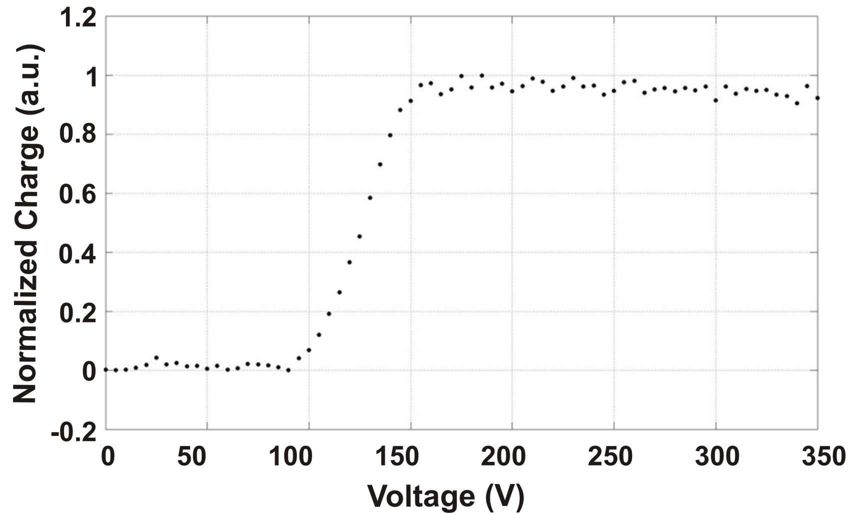

181 **Figure 9**. Collected charge versus the reverse voltage for the standard microstrip PiN N on P detector.

182 Using this shape analysis technique, the signal amplification on a full-fledged iLGAD
183 detector (microstrip P on P LGAD) has been observed for the first time, as shown in Figure 8.
184 In this case, the peaks of the weighting and the electric fields do not overlap and, as a
185 consequence, the waveform presents a horns-like shape, being the first pole induced by the drift
186 of primary electrons and the second pole dominated by the drift of secondary holes generated by
187 impact ionization effect thus demonstrating the gain of the new microstrip iLGAD detector.

188 At the first pole, the laser-created primary electrons drifting from the segmented P^+ side
189 towards the non-segmented multiplication side mostly induce the current. Then (at 12 ns)
190 electrons reach the multiplication P-type diffusion and the drift of the secondary holes towards
191 the segmented P^+ side starts (second pole). The weighting field peak is located near the P^+
192 diffusion while the electric field peak is located at the multiplication junction, leading to the
193 horn-like shape.
194

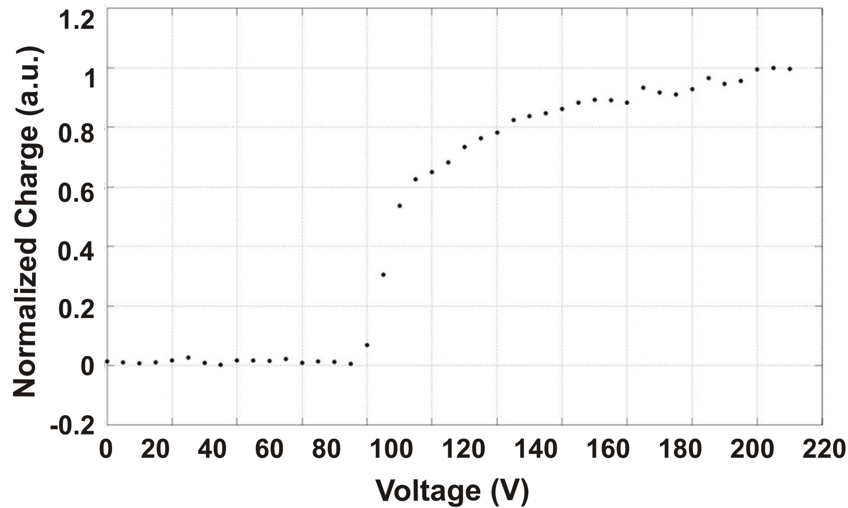

195
196
197 **Figure 10**. Collected charge versus the reverse voltage for the microstrip LGAD N on P detector.

198 In addition to the current waveform analysis, the dependence between the amount of
199 collected charge and the applied reverse voltage has also been measured. This dependence is
200 plotted in Figure 9 for the standard microstrip PiN N on P detector and in Figure 10 for the
201 microstrip LGAD N on P detector. As expected, once the detectors are completely depleted the
202 microstrip LGAD detector still increases the collected charge with the reverse voltage.

203 ## 6. Conclusions

204 The paper describes the design, optimization, fabrication and electrical performance of the
205 microstrip iLGAD detectors addressed to tracking and timing in moderate radiation
206 environments, primary vertex interaction and medical applications. The segmentation of the P^+
207 diffusion instead of the multiplication region provides a uniform electric profile and gain
208 wherever the incident particle hits the detector, solving the main drawback of the microstrip
209 LGAD counterparts where gain is only found at the centre of the strips. TCAD simulations of
210 electric field distribution, gain and transient current collection have been used for the
211 optimization of the iLGAD structure. The first fabricated microstrip iLGAD prototypes exhibit
212 a leakage current as low as the microstrip LGAD with a voltage capability in the range of 900
213 V. Finally, the Transient Current Technique (TCT) has been used to corroborate the charge
214 collection capability of the fabricated prototypes where both electrons and holes contribute to
215 the detection current. Signal amplification has been observed in iLGAD structures for the first
216 time.

217 ## Acknowledgments

218 This work was developed in the framework of the CERN RD50 collaboration and financed by
219 the Spanish Ministry of Economy and Competitiveness through the Particle Physics National
220 Pro- gram (FPA2013-48387-C6-1-P, FPA2014-55295-C3-2-R, FPA2015-71292-C2-1-P, and
221 FPA2015-69260-C3-3-R). This project has received funding from the European Union's
222 Horizon 2020 Research and Innovation program under Grant Agreement no.654168 (AIDA-
223 2020) and co-financed with FEDER funds. The authors would like to thank Dr. Evangelos
224 Leonidas Gkougkousis for his help in the SIMS measurements.

225 ## References

226 [1] G. Lutz, *Semiconductor Radiation Detectors: Device Physics*, Springer Editor, 2007.
227 [2] G. Pellegrini et al., *Technology Developments and First Measurements on Low Gain Avalanche*
228 *Detectors (LGAD) for High Energy Physics Applications*, Nucl. Instrum. Meth. **A 765** (2014) 12.
229 [3] P. Fernández-Martínez et al., *Design and Fabrication of an Optimum Peripheral Region for Low*
230 *Gain Avalanche Detectors*, Nucl. Instrum. Meth. **A 821** (2016) 93.
231 [4] G. Kramberger et al., *Radiation Effects in Low Gain Avalanche Detectors After Hadron*
232 *Irradiations*, Journ. of Instr. **10** (2015).
233 [5] M. Carulla et al., *The HGTD: A SOI Power Diode for Timing Detection Applications*, Int. Sem. on
234 Power Semicond., Prague (2016).
235 [6] G. Pellegrini et al., *Recent Technological Developments on LGAD and iLGAD Detectors for*
236 *Tracking and Timng Applications*, Nucl. Instrum. Meth. **A 831** (2016) 24.
237 [7] V. Eremin et al., *Development of transient current and charge techniques for the measurement of*
238 *effective net concentration*, Nucl. Instrum. Meth. **A 372** (1996) 388.
239 [8] G. Kramberger, *Advanced Transient Current Technique Systems,* PoS (Vertex2014) 032.